Electronic Research Archive

http://www.aimspress.com/journal/era

ERA, 32(4): 2936–2954.
DOI: 10.3934/era.2024134
Received: 29 December 2023
Revised: 19 March 2024
Accepted: 09 April 2024
Published: 16 April 2024

Research article

An interpretable mechanism for grating-induced cross-inhibition and gamma oscillation based on a visual cortical neuronal network model

Hao Yang[1], Peihan Wang[1], Fang Han[1,*] and Qingyun Wang[2]

[1] College of Information Science and Technology, Donghua University, Shanghai 201620, China
[2] Department of Dynamics and Control, Beihang University, Beijing 100191, China

* **Correspondence:** Email: yadiahan@163.com.

Abstract: Biological experiments targeting the mammalian primary visual cortex have shown that neuronal response to a preferred orientation grating is cross-inhibited by an orthogonal orientation mask grating. The plaid formed by the overlap of the two gratings not only causes a decrease in the neuronal firing rate but also shifts the gamma oscillation to a weaker oscillation at a higher frequency. The mechanism for the above phenomena is unclarified. In this paper, a large-scale cortical neuronal network model with biological details is constructed. In this model, two modes of connectivity that may contribute to cross-inhibition are considered: the thalamo-cortical feedforward pathway and the push-pull organization of cortical layer 4. Based on this model, the modulation of firing rate and gamma oscillation by a plaid stimulation are successfully reproduced, which is consistent with biological experiments and suggests that it is the thalamo-cortical feedforward pathway that leads to cross-inhibition. Furthermore, our analysis of the neuronal spike clusters and current fluctuations suggests that the push-pull organization leads to an increase in gamma frequency during the transition of visual stimuli from grating to plaid by modulating the source of synaptic inhibition in local neuronal populations. Such results will help to understand the visual processing under multi-input integration.

Keywords: primary visual cortex; cross-inhibition; gamma oscillation; push-pull organization; computational model

1. Introduction

Neurons in the primary visual cortex (V1) show cross-inhibition: sinusoidal gratings in the preferred orientation provide a strong synchronized feed-forward drive to the neurons, resulting in strong neural responses, but when gratings orthogonal to the preferred orientation are presented at the same time to form a plaid, the neurons firing is significantly suppressed, even though this orthogonal grating causes almost no reaction when presented alone [1–4]. At the same time, the plaid will increase the firing rate

of the other neurons, as the additional gratings will be closer to their preferred orientation [5–7]. In addition, some non-orientation-tuned V1 neurons respond strongly to plaids [8, 9]. How do neurons combine responses in one-dimensional directions to characterize two-dimensional composite patterns? What is the structure of the neural circuit for this combination? Explaining these questions could help us better understand visual processing processes. The local-field potential (LFP) in V1 can also be observed to exhibit gamma oscillation when grating stimuli are presented, and the properties of gamma oscillation depend on the grating parameters. When superimposed with orthogonal gratings forming a plaid, the strong and sustained gamma oscillation induced by such gratings is transformed into a weaker oscillation at a higher frequency [6, 10–12]. It is widely accepted that gamma oscillations are important indicators of neural processing related to visual perception and cognition and play an important role in visual stimulus representation, selection, processing, and transmission [13–17], but how gamma oscillations vary with plaid has not been systematically investigated.

The source of cross-inhibition in V1 remains controversial, with the prevailing views being cortical synaptic inhibition dominance [11, 18, 19], feedforward dominance [3, 9, 20], or a combination of the two [21, 22]. For example, Priebe and Ferster [3] found in intracellular recordings from simple cells that orthogonal stimuli inhibited both synaptic inhibition and synaptic excitation, suggesting that cross-inhibition does not arise from synaptic inhibition between populations with different orientation preferences. In contrast, Perry [11] failed to find evidence of cross-orientation inhibition in the initial pattern of onset-evoked responses, which contradicts the idea that cross-inhibition originates from feedforward inputs. At the same time, numerous models have been proposed to simulate and explain this phenomenon: Koelling et al. [22] demonstrated that a model incorporating retinal contrast gain control and inhibitory cortical networks could account for the phenomenon of cross-inhibition; Carandini et al. [23] and Heeger et al. [24] used the normalization model to simulate the suppression effect after the appearance of the second grating, since in this strategy, any increase in the contrast of either grating increases the normalization factor. The stabilized supralinear network (SSN) of Rubin et al. [19] relies on intracortical suppression to account for cross-inhibition while successfully modeling the facilitation of the firing rate by the superposition of two low-contrast gratings. Barbera et al. [20] reproduced the multiple effects of plaid modulation with a feedforward model and demonstrated that the heterogeneity of neuronal responses to plaids can be explained by interactions between stimulus geometry and orientation tuning without the need for intracortical interactions. The above studies can model and explain a wide range of neural phenomena, including cross-inhibition, but the network structure of these computational models rarely includes biological details, making it difficult to reflect the real intracortical situation.

As for gamma oscillation, some studies have shown that gamma and multi-unit activity (MUA) response patterns can be simultaneously fitted by normalized models [12, 25]. And Wang et al. [12] concluded that the neural mechanisms of gamma inhibition and firing activity are different. There has been a wealth of modeling work for gamma oscillations. A lot of network modeling work has simulated and explained the modulation of gamma oscillation by grating parameters such as angle, contrast, temporal frequency, and size [24, 26–29]. The modulation of gamma oscillation by different neural elements such as feedforward, feedback, lateral connections, and neuron types has also been explored [30–33]. However, modeling work related to superimposed gratings is still lacking, let alone the explanation of how and why the properties of gamma oscillation vary with superimposed grating parameters.

In this paper, we build a large-scale V1 cortical neural network with biological features to simu-

late the gamma oscillation and cross-inhibition induced by superimposed gratings. The model is built on anatomical data from a cat's primary visual cortex; a biologically realistic approach to converting drifting sinusoidal grating stimuli into neural activity is adopted; and two practical connectivity modes, the thalamo-cortical feedforward pathway and the push-pull organization of layer 4 (L4) [34–36], that may act on cross-inhibition, are considered. The model successfully simulates the inhibition of firing and the high-frequency low-power transition of the gamma oscillation after the superposition of orthogonally oriented gratings. Furthermore, the simulation results show that cross-inhibition originates from the feed-forward inputs, and the push-pull organization does not affect the magnitude of inhibition. Through individual-specific neuronal firing analyses and biologically realistic connectivity patterns, we provide new insights into the mechanisms behind plaid modulation of the gamma oscillation in V1: the push-pull organization leads to an increase in gamma frequency during the transition of a visual stimulus from grating to plaid through modulation of the source of synaptic inhibition in a local population.

2. Materials and methods

To simulate the plaid-induced gamma oscillation and cross-inhibition, we built a large-scale V1 model as shown in Figure 1. The model corresponds to the visual information pathway in which visual stimuli reach L4 of V1 via the lateral geniculate nucleus of the thalamus. LGN neurons provide excitatory feedforward inputs to L4 neurons based on specific visual stimuli, and L4 contains 8000 excitatory neurons and 2000 inhibitory neurons, with neuronal connectivity determined by distance, type, and receptive field. A detailed description of the model is shown in the following sections.

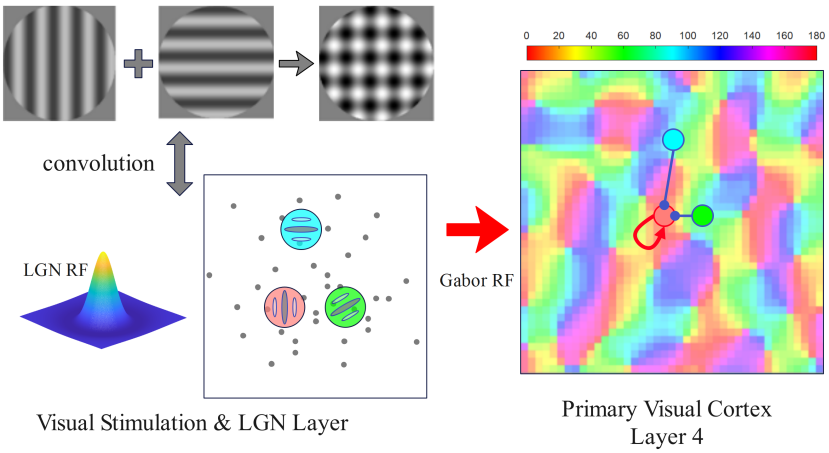

Figure 1. Model structure. Visual stimuli are convolved with the LGN receptive field to obtain the LGN input current, and cortical neurons receive feedforward inputs from the LGN layer according to their respective Gabor receptive fields, with the Gabor receptive fields corresponding one-to-one with the L4 example neurons in the figure; L4 neuronal connectivity follows the push-pull organization, so that excitatory inputs to the vertical preference population (red circle) come from itself, with a portion of inhibitory inputs coming from the neighboring populations (blue and green circles).

2.1. Visual stimuli

In this paper, the visual stimulus is a plaid pattern formed by the superposition of two mutually orthogonal drifting sinusoidal gratings, with the luminance g of a single grating pixel point defined as:

$$\begin{aligned} g(x,y,t,c,o) &= l\left(1+c\cdot\sin\left(2\pi f_s\theta(x,y)+2\pi f_t t\right)\right) \\ \theta(x,y) &= \sin(\pi/2-o)\,x+\cos(\pi/2-o)\,y, \end{aligned} \tag{2.1}$$

where $g(x,y,t,c,o)$ is the luminance of a grating with contrast c and orientation o at position (x,y) and moment t, the background luminance $l = 50$, the spatial frequency $f_s = 0.8$, and the temporal frequency $f_t = 4$. In the following simulation, we define the vertical primary grating g_1, which evokes strong neuronal activity, and the horizontal secondary grating g_2, which serves as a mask. When they superimpose, $g_{\text{plaid}} = g_1 + g_2 - l$. That is, the luminance of the corresponding pixels of the two gratings is summed, and then the background luminance is subtracted. The contrast c_1 of the primary grating is always 50%, and the mask contrast of the secondary grating c_2 is between 0 and 50%. When $c_2 = 0$, this corresponds to the case where only the primary grating g_1 is presented. A constant value of g_{plaid} is presented in each experiment, and c_2 is the main variable of the plaid across experiments.

2.2. LGN layer

LGN neurons are mediators of visual stimuli to V1, divided into two types, ON-center and OFF-center, which are sensitive to bright areas surrounded by shade and shade areas surrounded by bright, respectively [37, 38]. The number of both types of neurons in this model is set as 450, randomly distributed within a 5 mm × 5 mm plane. The only role of LGN layer neurons is to provide excitatory feedforward inputs to cortical neurons, and there are no synaptic connections between them. Based on the work of Kremkow et al. [35], neurons are modeled as the g'wegrate-and-firegw model: $C_m\frac{dV}{dt} = -g_L(V-E_L)+I_{in}, C_m = 0.29, g_L = 0.029, E_L = -70$ mV, the refractory period is 2 ms. The input current I_{in} is obtained by convolving the receptive field with the stimulus movie, where the ON center neuron receptive field RF_{ON} is defined as [37]:

$$\begin{gathered} RF_{\text{ON}}(x,t) = F_c(x)\,G_c(t) - F_s(x)\,G_s(t) \\ F_c(x) = A_c\exp\left(-\tfrac{x^2}{2\sigma_c^2}\right), F_s(x) = A_s\exp\left(-\tfrac{x^2}{2\sigma_s^2}\right) \\ G_c(t) = K_1\frac{(c_1(t-t_1))^{n_1}\exp(-c_1(t-t_1))}{n_1^{n_1}e^{-n_1}} - K_2\frac{(c_2(t-t_2))^{n_2}\exp(-c_2(t-t_2))}{n_2^{n_2}e^{-n_2}} \\ G_s(t) = G_c(t-td). \end{gathered} \tag{2.2}$$

The specific parameter settings refer to Allen and Freeman [37]. For OFF center neurons, the receptive field $RF_{\text{OFF}} = -RF_{\text{ON}}$.

2.3. Cortical neuron model

We mainly model L4, which is the input layer in V1, and it covers a 5° × 5° field of view with 8000 excitatory and 2000 inhibitory neurons randomly distributed on a 3 mm × 3 mm plane. Considering the biological details as well as the simplicity and ease of computation of the model, the single-compartment exponential integrate-and-fire (Exp-IF) model is chosen to model cortical neurons. Exp-IF neurons add an exponential term $\Delta_T\exp\left((V-V_T)/\Delta_T\right)$ to integrate-and-fire (IAF) neurons. Fourcaud-Trocmé et al. [39] have demonstrated that the firing rate response to constant or noisy

currents of the Exp-IF model is closer to the Wang-Buzsáki (WB) model in a broad range of firing rates than the IAF neuron model and other variations of the IAF model. Moreover, the subthreshold membrane potential trajectories of the Exp-IF model and the WB model are almost indistinguishable, and the I-V curves are very similar near the threshold voltage because the activation curve of the fast sodium current in the WB model can be well approximated by the exponential term. The time course of the membrane potential $V(t)$ of an Exp-IF neuron is:

$$\tau_m \frac{dV}{dt} = -(V - E_L) + \Delta_T \exp\left(\frac{V - V_T}{\Delta_T}\right) + w_{\text{exc}}(E_{\text{exc}} - V) + w_{\text{inh}}(E_{\text{inh}} - V), \tag{2.3}$$

where w_{exc} and w_{inh} are the excitatory and inhibitory synaptic weights, respectively. When the membrane potential v crosses the threshold $V_T = -53$ mV, the neuron fires and resets the membrane potential to the resting value $V_r = -70$ mV. The time constants τ_m of excitatory(E) neurons and inhibitory(I) neurons are 10 ms and 15 ms, respectively, and the refractory periods are 2 ms and 0.5 ms, respectively. Other parameters are set as $E_L = -70$ mV, reversal potentials $E_{\text{exc}} = 0$ mV, and $E_{\text{inh}} = -80$ mV. The values of the threshold slope factor $\Delta_T = 0.8$ mV are taken to fit the pyramidal neurons [38]. The spatial location of a neuron determines its orientation preference property [40]. In this paper, we place a population containing 200 vertical preference neurons at the center, and our study will focus on this population.

2.4. Synaptic connection probability

Binzegger et al. [41] have developed a quantitative description of the circuits formed in cat V1. When only the internal connections of layer 4 are considered, the number of excitatory synaptic inputs received by both E neurons and I neurons accounts for 65% of the total number of synaptic inputs. However, L4 neurons receive a large amount of excitatory input from L6, and when this component is taken into account, 79.4% of the synapses received by E neurons are excitatory, and for I neurons, it is 82.9%. We, therefore, specify that each E neuron receives 800 synaptic inputs and each I neuron receives 640 synaptic inputs due to its smaller size, of which 80% are excitatory (10% from the LGN layer, 70% from the E neurons) and 20% are inhibitory. After determining the number of synapses, the connection probability has to be specified. For each neuron, we reproducibly sample the inputs from potential presynaptic neurons according to a certain probability distribution. Strategies for calculating the probability of different types of synaptic connections are presented as follows:

The shape of a cortical neuron's receptive field determines the arrangement of the LGN neurons that provide feed-forward inputs, which in turn determines their orientation preference. In this paper, we model the cortical neuron's receptive field with the Gabor distribution [34]:

$$\begin{aligned} g(x, y, \theta, \psi) &= \exp\left(-\frac{x'^2 + y'^2\gamma^2}{2\sigma^2}\right)\cos(2\pi x'\lambda + \psi) \\ x' &= x\cos\theta + y\sin\theta \\ y' &= -x\sin\theta + y\cos\theta, \end{aligned} \tag{2.4}$$

where g is the connection probability, (x, y) is the difference in coordinates of the pre- and post-synaptic neurons, θ is the preferred orientation of the post-synaptic neuron, and ψ is the preferred phase, which is randomly set in this paper [38]. Other parameters are set as $\sigma = 0.17, \lambda = 0.8, \gamma = 2.5$. Positive and negative regions of Gabor correspond to connections from ON and OFF-center feedforward neurons, respectively.

The probability of connection between L4 neurons is determined by distance d and push-pull organization (determined by the correlation c of their receptive fields). First, the connections formed by L4 neurons are mostly localized, and Antolik et al. [38] fit the anatomical data from Stepanyants et al. [42] with the zero mean hyperbolic distribution, i.e., $g_{\text{dist}}(d)$. Meanwhile, L4 neurons follow a push-pull organization in generating connections, with excitatory and inhibitory neurons preferentially connecting with neurons with correlated and anti-correlated Gabor receptive fields, i.e., $g_{\text{push - pull}}(c, d)$ [34–36,38]. The final probability is calculated as the multiplication of the two components:

$$\begin{aligned} g(c,d) &= g_{\text{push - pull}}(c) \cdot g_{\text{dist}}(d) \\ g_{\text{push - pull}} &= \frac{1}{\sigma\sqrt{2\pi}} \exp\left(-(c-\mu)^2/2\sigma^2\right) \\ g_{\text{dist}}(d) &= \exp\left(-\alpha\sqrt{\theta^2+d^2}\right), \end{aligned} \tag{2.5}$$

where α and θ in distance components g_{dist} depend on the type of synapse: $\alpha = 0.0139, \theta = 207.7$ for synapses from E neurons to E neurons; $\alpha = 0.0148, \theta = 191.8$ for synapses from E neurons to I neurons; $\alpha = 0.0126,\ \theta = 237.5$ for synapses from I neurons to E neurons; and $\alpha = 0.0119,\ \theta = 256.4$ for synapses from I neurons to I neurons. In the push-pull component $g_{\text{push-pull}}$, the correlation c is related to both the orientation and the distance of the receptive fields: for two receptive fields, the larger the distance, the smaller the correlation; the correlation is positive when the gap between the orientations is small, and the correlation is negative when the orientations are almost orthogonal [34, 38]. μ takes 1 and -1 for excitatory and inhibitory synapses, respectively. The smaller σ indicates the stronger push-pull effect, and it is set as 1.4 in the initial simulation, which will be modified in subsequent experiments.

2.5. Synaptic model

The time evolution of synaptic weights is modeled as an exponential difference model of AMPA, NMDA, and GABA types [43, 44]. The time course of inhibitory synaptic weights for neuron n in Eq (2.2) is defined as:

$$\begin{aligned} w_{\text{inh},n}(t) &= \sum_{\sigma} w_{\sigma} \sum_{m\in\text{Pre}} \sum_{j=1}^{k} G_{\text{GABA}}\left(t - \left(t_{j,m} + t_{\text{delay}}\right)\right) \\ G_{\text{GABA}}(t) &= \frac{\exp\left(-t/\tau_{d,\text{GABA}}\right) - \exp\left(-t/\tau_{r,\text{GABA}}\right)}{\tau_{d,\text{GABA}} - \tau_{r,\text{GABA}}}, \end{aligned} \tag{2.6}$$

where σ is the presynaptic neuron species, w_{σ} is the basic weight, Pre is the set of presynaptic neurons, and k is the number of spikes that have been generated by neuron m. Neuron m produces the jth spike at moment $t_{j,m}$ and affects the synaptic weight of neuron n after a delay of t_{delay}. $G_{\text{GABA}}(t)$ describes the time course of synaptic weights when the fire of neuron n is transmitted to neuron m at moment 0, τ_r is the rise time constant, and τ_d is the decay time constant. AMPA and NMDA synapses are defined similarly. The excitatory synaptic weight G_{exc} contains both AMPA and NMDA components. The percentage of AMPA is 0.8 when the postsynaptic neuron is an E neuron and 0.67 when it is an I neuron. The rise and fall time constants for GABA-type synapses are 2 ms and 3 ms, respectively; for AMPA-type they are 0.5 ms and 2 ms; and for NMDA-type are 2 ms and 40 ms.

Synaptic delay is proportional to distance: $t_{\text{delay}}(x) = ax + b$, where $a = 10/3$, and b is related to synapse type. The values are 1 for inhibitory synapses, 1.4 for synapses from E neurons to E neurons, and 0.5 for synapses from E neurons to I neurons [38]. The synaptic basic weights in Eq (2.3) are set as follows: 0.08 for E neurons accepting feedforward inputs, 0.04 for I neurons accepting feedforward inputs, 0.05 for synapses from E neurons to E neurons, 0.08 for synapses from E neurons to I neurons, 0.20 for synapses from I neurons to E neurons, and 0.14 for synapses from I neurons to I neurons. Under the current network structure, the above parameter settings will ensure that the model produces fire activity consistent with biological reality.

2.6. PSD analysis

The local-field potential (LFP) is an easily accessible measure of the activity of local neuronal populations that primarily reflects the synaptic activity of excitatory neurons [45–48]. In most studies on gamma oscillation, LFP signals are used for spectral analysis. The traditional modeling approach is to consider the membrane potential of the central E component as the LFP because the membrane potential fluctuation of the central E component responds to the activity of other E components in the local region [26, 28]. Mazzoni et al. [49] argue that the weighted sum of AMPA currents and GABA currents in the LIF network responds well to the time course of the LFP signal. Other than that, Rangan and Young [50] propose that "multiple firing events (MFEs)" affect the gamma oscillation of the LFP: during an MFE, the net synaptic effect of the firing population significantly reduces the subthreshold voltage of the non-firing population, and these lowered membrane potentials are elevated during the interval between MFEs. The similarity between the analyses for MFEs and LFPs in the gamma band has been confirmed in related modeling studies [44, 51].

Because of the similar model structure, we adopt the MFE analysis, and SD is a measure of MFE. Due to the similarity of the models, the same method as Chariker et al. [44] is chosen, i.e., power spectral density (PSD) analysis of the spike density (SD), an important parameter for determining the MFEs. The SD is defined as the ratio of all spikes in the neuron population to the total number of neurons in the population within a time bin. Consider the firing activity of a population containing N neurons during the period $(t, t + T)$, divide this period equally into $n = T/\Delta t$ time windows, define the total number of discharges in the ith time window B_i as m_i, and then the SD within B_i is defined as $d_n = m_n/(N\Delta t)$. In this way, the PSD of SD is defined as:

$$\hat{d}(f) = \frac{1}{\sqrt{T}} \sum\nolimits_{n=1}^{T/\Delta t} d_n \Delta t \exp\left(-2\pi i f n \Delta t\right). \tag{2.7}$$

We set $T = 200$ ms and $\Delta t = 4$ ms, and the periods are set as $(0, T), (\Delta t, \Delta t + T), ..., (n\Delta t, n\Delta t + T)$.... The sliding time bins allow us to obtain the temporal evolution of gamma oscillations, but at this stage we mainly consider PSDs averaged over time. We consider the peak frequency and spectral power of gamma oscillations, where the peak frequency is the frequency corresponding to the maximum power and the spectral power is calculated as the summed power in the range of 30–80 Hz [26].

3. Results

3.1. Neuronal response modulated by the orthogonal mask grating

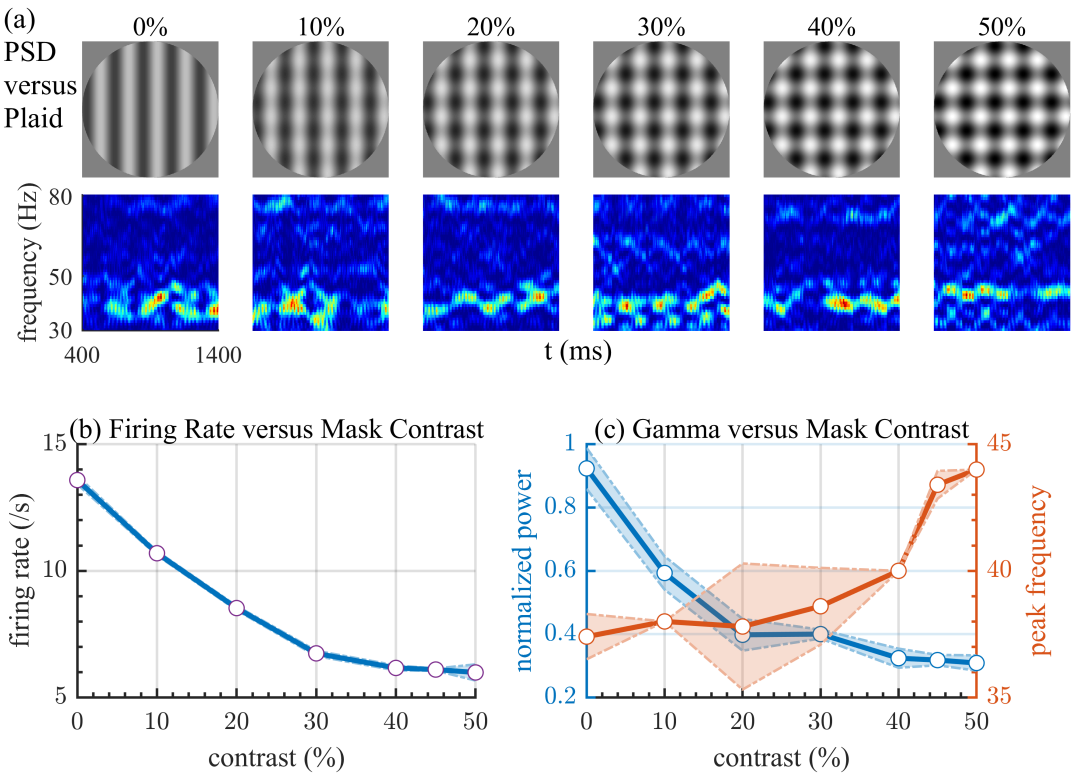

Figure 2. Firing activity with grating and plaids as visual stimuli. (a) Oscillatory PSD analysis of vertical preference populations at different contrasts of horizontal mask gratings. (b) Cross-inhibition during contrast enhancement of horizontal mask gratings. (c) Band power (blue line on the left axis) and peak frequency (red line on the right axis) of gamma oscillation modulated by horizontal grating contrast. The solid line stands for the average of five independent experiments, while the light-colored area surrounded by the dotted line shows the standard deviation.

Numerous biological experiments have summarized the effect of grating superposition on the response of V1 neurons: the superposition of mask gratings leads to a decrease in the firing rate of the majority of neurons, i.e., cross-inhibition, as compared to the primary grating when presented alone [2, 3, 7]. At the same time, the strong and sustained gamma oscillations induced by the main grating shift to weaker oscillations at a higher frequency [6, 10–12]. We have successfully simulated these phenomena in our model: When a vertically drifting sinusoidal grating with 50% contrast is presented as a visual stimulus, the vertically preferred neuron population produces continuous and strong synchronized oscillation in the gamma band. In this population, the average discharge rate is 13.7/s, and the peak frequency of gamma oscillations is 37 Hz. Based on this, we further select a horizontal mask grating with a contrast of 10% to 50% to superimpose on the original grating. With the increasing

contrast, the stability of gamma oscillation decreases, with significant differences in peak frequency between the 20% and 40% ranges, while the oscillation becomes weaker but relatively stable when the contrast is greater than 40%, as shown in Figure 2(a). The results show that the rise in contrast of the mask grating leads to a decrease in the firing rate, as shown in Figure 2(b), a decrease in the gamma band power, and an increase in the peak frequency, as shown in Figure 2(c). When the contrast of the two gratings is equal, the appearance of the mask grating decreases the firing rate by 60% and the band power by 70%, while the peak frequency increases from 37 Hz to 44 Hz.

3.2. Cross-inhibition in this model originates from the feed-forward pathway

It is generally accepted that synaptic inhibition within the cortex and feed-forward inputs lead to cross-inhibition, so the two aspects of the model are discussed in this section.

Feedforward inputs to neurons in this model come from LGN neurons, which receive excitatory inputs from visual stimuli via a spatiotemporal receptive field based on the difference of Gaussian; an individual LGN neuron does not have an orientation preference, whereas the spatial distribution of thalamo-cortical connections determines the preferred orientation of cortical neurons. We consider an ideal situation and set 21 LGN neurons with receptive field centers on a vertical line to provide feed-forward inputs to a vertically preferred cortical neuron and probe the responses of the LGN and cortical neurons with a vertical grating, a horizontal grating, and the plaid formed by overlapping them as stimuli, respectively. An LGN neuron is randomly selected, and its input current is plotted, which shows that the input current to LGN neurons under sinusoidally drifting grating stimulation also exhibits the sinusoidal waveform (see Figure 3(a)), so we mainly consider the current peak. Since there is no orientation preference for a single LGN neuron, the magnitude of currents triggered by gratings of two orientations is equal, whereas the magnitude of currents under plaid stimulation varies with the grating phase, and the peaks are smaller than the single grating case at most positions (see Figure 3(b)). There is no phase difference between the two gratings at the center, but there is limited current growth in this LGN neuron. This is due to the fact that the LGN neuron receptive field possesses the Difference of Gaussian (DOG) structure (see Eq (2.2)): after the superposition of orthogonal gratings, while the luminance of the positive region in the center of the receptive field increases, the luminance of the surrounding negative region increases as well, and the two counteract each other, resulting in a small current rise. Concurrently, the synaptic weight of V1 neurons under the three stimuli shows a large difference (see Figure 3(c)). The stripe orientation of the vertical gratings matches the arrangement of the LGN neurons, resulting in strong synchronization of their spikes, which instantaneously provide large inputs to the cortical neurons and trigger intense firing activity (see blue lines in Figure 3(c)). Although the horizontal grating causes single LGN neurons to produce the same firing rate, presynaptic neurons fire sequentially in alternating light and dark stripes, providing a constant small input current to the cortical neurons, thus leading to weak firing activity, which underlies the generation of the orientation preference in the model (see red lines in Figure 3(c)). The current under plaid stimulation is slightly stronger than the horizontal grating, but still not enough to allow the cortical neurons to obtain a high firing rate (see yellow lines in Figure 3(c)). In the actual model, the LGN neurons are more widely and randomly distributed; thus, the feedforward pathway is sufficient to produce significant cross-inhibition.

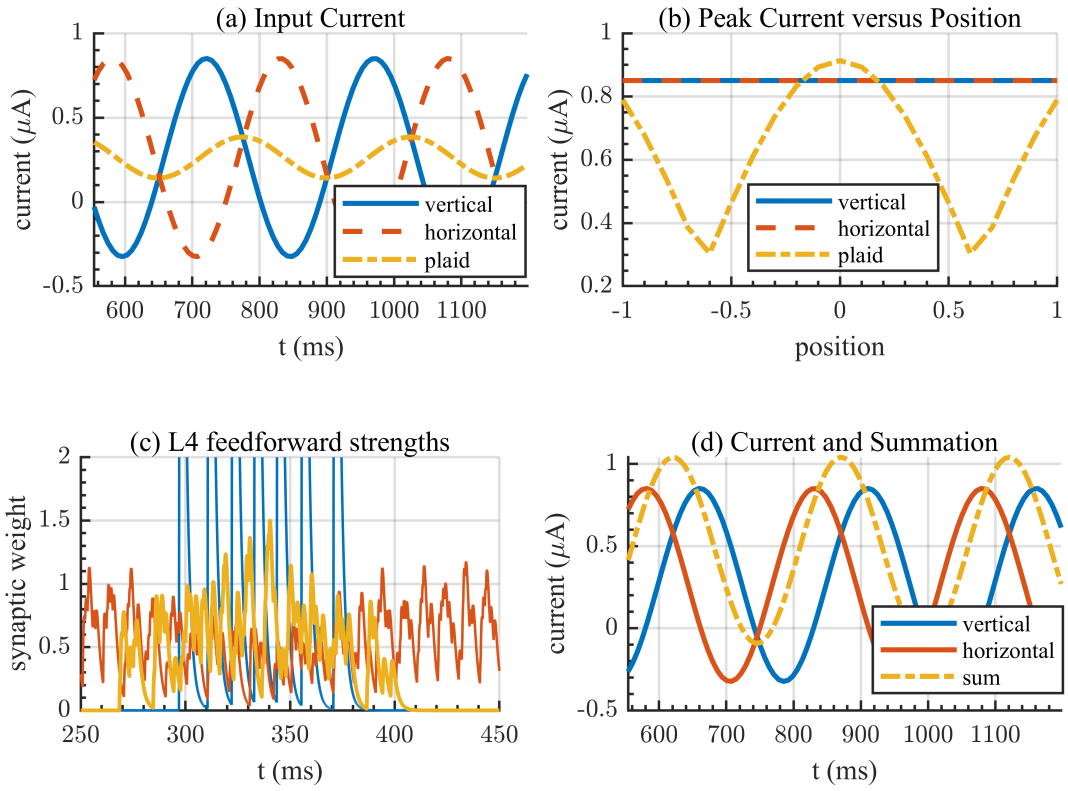

Figure 3. Changes in LGN neuron input current and cortical feedforward weights under three types of stimuli in the ideal model consisting of 21 LGN neurons lined up in a straight line and cortical neurons receiving feedforward input from them (blue: vertical grating, red: horizontal grating, yellow: two gratings superimposed to form a plaid). (a) Input currents to a randomly selected LGN neuron. (b) The maximum value of sinusoidal current fluctuations for all 21 LGN neurons in terms of position as a horizontal coordinate. (c) The synaptic weight changes of the cortical neuron. (d) Modified the current calculation strategy to eliminate cross-suppression from the feedforward.

In L4 of this model, the push-pull organization determines that excitatory and inhibitory neurons preferentially make connections with neurons that possess correlated and anti-correlated Gabor receptive fields [34–36]. Neurons preferring similar orientations in the layer cluster into populations, whereas neighboring populations differ greatly in preferred orientations [40, 52]. This determines that the excitatory connections of a particular cluster come primarily from itself, while the inhibitory connections come from other nearby populations. The stronger the push-pull effect, the more specific the source of such excitatory-inhibitory connections. In order to explore the effect of the push-pull organization on cross-inhibition, i.e., whether the appearance of the orthogonal grating suppresses the firing of neurons in the local population by increasing the firing rate of the surrounding orthogonal preference population, the superposition strategy of gratings is modified here: instead of letting the two gratings be presented simultaneously, the sum of the LGN input currents generated by the two gratings is calculated individually (see Figure 3(d)). The results show that when there is no connection within the

cortex, the firing rates of the vertically-preferred and horizontally-preferred populations are identical and close to the level when a single vertical grating is presented, and the cross-inhibitory effect of the feed-forward is eliminated, suggesting that cross-inhibition caused by the feed-forward is eliminated.

The strength of the push-pull effect (push-pull strength) in this model is determined by σ in Eq (2.5), and the larger the σ, the weaker the push-pull effect. Here we consider the cases with the value of σ being 1, 1.4, 2, and no push-pull effect (denoted as inf), respectively. The results show that the grating-induced firing rate is slightly higher than that induced by the plaid, and as the push-pull effect becomes weaker, the grating- and plaid-induced firing rates decrease almost synchronously, and no obvious suppression occurs (see Figure 4). When no push-pull organization exists, the plaid firing rate is 70% of the grating, whereas the ratio increases to 90% for $\sigma = 1$, suggesting that the overpowering push-pull even obstructs cross-inhibition. This is due to the fact that with the current parameter settings, push-pull organization similarly enhances excitatory current connections within the population, and this enhancement is sufficient to counteract the inhibitory effects from other neuronal populations. The sharp rise in the firing rate when σ changes from 1.4 to 1 also results from this. The decrease in firing rate due to the plaid in the absence of push-pull similarly suggests that push-pull organization is not a necessary condition for cross-inhibition in this model, which is consistent with Priebe and Ferster [3] that synaptic inhibition between neurons with different preferred orientations is not responsible for cross-inhibition.

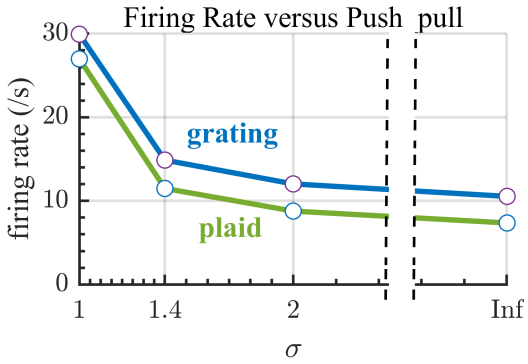

Figure 4. Changes in firing rate when 50% vertical grating (blue) and 50% vertical + 50% horizontal grating superimposed plaid (green) are used as visual stimuli, respectively, when the push-pull strength varies after eliminating feed-forward factors.

3.3. Push-pull organization leads to the increase of gamma frequency

The appearance of the horizontal mask grating and its contrast enhancement lead to a decrease in the gamma band power and an increase in the peak frequency of the vertical preference population. Both the difference in the moment of feedforward current arrival and the decrease in cortical neuron firing rate presented in Figure 3(c) lead to difficulties in maintaining synchronized firing within the population, thus decreasing gamma band power. As for the frequency, rapid excitation and delayed inhibition in the EI network are alternating [53, 54], and it is questionable how the inhibited firing activity can achieve rapid state transitions to generate a larger oscillation frequency. In this part, by

adjusting the push-pull strength, we prove that it is the push-pull organization that shapes this trend in the oscillation frequency.

We consider a 50% vertical grating stimulus and a plaid stimulus formed by the superposition of two 50% orthogonal gratings, adjusting σ within 1.2 to 2.0, which does not overly affect the original firing rate. The results in Figure 5(a) indicate that the peak frequency under plaid stimulation is always stabilized at 44 Hz, with no fluctuation even in multiple independent simulations, while on the contrary, the peak frequency under grating stimulation gradually rises from 38 Hz to 44 Hz with decreasing push-pull strength, with a large disparity between simulations. That is, the push-pull organization causes a relative increase in gamma oscillation frequency under plaid stimulation by decreasing the oscillatory frequency of the second grating.

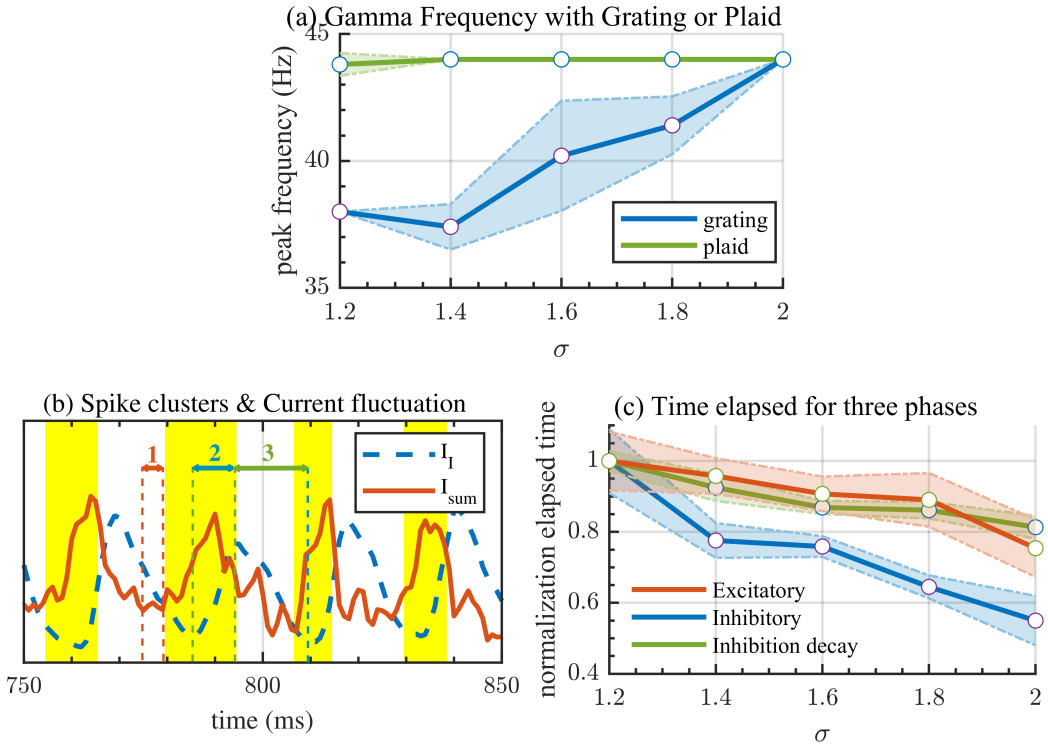

Figure 5. Modulation effect of push-pull strength on peak frequency of gamma oscillation. (a) The trend of peak frequency changes when 50% vertical grating (blue) and 50% vertical + 50% horizontal grating superimposed on plaid (green) are the stimuli. (b) Relationship between firing cluster events (yellow bars) and fluctuations in normalized input currents (blue: inhibitory current; red: total current) of E neurons. The three phases are identified by arrows and numbers in the corresponding colors. (c) Change in elapsed time (normalized) for the excitation phase (red), the inhibition phase (blue), and the inhibition decay phase (green) of the network when 50% vertical grating is used as the visual stimulus. The solid line in (a) and (c) stands for the average of five independent experiments, while the light-colored area surrounded by the dotted line shows the standard deviation.

To quantify this frequency variation, we first define spike clustering events as a period in which the

total number of spikes within the population at each moment is greater than one-half of the expected value [50, 51]. Next, by analyzing the spike clusters and population-normalized input currents, we define three phases for each gamma cycle that most affect the oscillation frequency (see Figure 5(b)): 1) Excitatory phase: the time since a small number of E neurons cross the threshold to shift the network from resting to active, corresponding to the phase when the total input current is minimized to the beginning of a spike cluster; 2) Inhibitory phase: the time since active I neurons inhibit the synchronized firing of the population, corresponding to the phase in which the I current within a spike cluster rises to the end of this spike cluster; 3) Inhibition decay phase: the time since the inhibition of E neuron activity leads to a decrease in excitatory input to I neurons and a decrease in overall inhibition within the population, corresponding to the I current decay phase.

In order to clarify the cause of the increase in the frequency of single grating-induced gamma oscillations due to the decrease in push-pull strength, we plotted the average elapsed time of these three phases as a function of σ in Figure 5(c). Because of the differences in the duration of the three phases, we normalized them to compare which phase had the most significant change. As shown in Figure 5(c), the elapsed time in the inhibitory phase (blue) decreases with increasing σ, i.e., decreasing push-pull strength, and the decrease is larger than that in the excitatory phase (red) and inhibition decay phase (green). This phenomenon suggests that neuronal populations become more easily inhibited with decreasing push-pull strength, resulting in an increase in oscillation frequency.

Initially, when the push-pull effect is strong, the central population is primarily inhibited by adjacent populations because inhibitory neurons under the push-pull organization prefer to connect neurons with anti-correlated receptive fields (i.e., different preference orientations). The stronger the push-pull effect, the more pronounced this tendency is. These adjacent populations do not prefer the orientation of a single grating and provide limited inhibition to the central population. As the strength of the push-pull effect (push-pull strength) diminishes, for central populations and adjacent populations with different preferred orientations, the weakening of push-pull strength results in more excitatory synapses from the central population connecting to the adjacent populations, and more inhibitory synapses from the central population connecting within the central population. This leads to a decrease in the activity of the central population, while adjacent populations become more active. This further leads to increased suppression from adjacent populations, while the central population is more susceptible to suppression, so that an increase occurs in the frequency of oscillations. This can likewise explain why the contrast enhancement of the mask grating leads to a rise in the oscillation frequency, i.e., the neural activity of the neighboring populations becomes stronger, enough to accelerate the suppression of the central population activity.

4. Discussion

Koelling et al. [22] similarly use LGN neurons with spatiotemporal receptive fields and IAF cortical neurons to model cross suppression, but they did not observe inhibition of the LGN response by the plaid pattern. This is due to the fact that the spatial frequency of their gratings is much larger and the grating stripes cover the entire receptive field rather than the positive regions in the receptive field, so that the superimposed gratings do not lead to the involvement of more negative regions of the receptive field, as in our work. The spatial frequency of gratings may affect the principle of cross-suppression generation, which needs to be taken into account in further work. The work of Rubin

et al. [19], Carandini et al. [23], and Heeger et al. [24] actually allows the two components of the plaid to act on neuronal populations with corresponding preferred orientations at the same time, rather than the two gratings being directly superimposed. This is certainly good practice when the effect of intracortical connectivity on cross-inhibition needs to be considered separately, since inhibition from neuronal populations with other preferred orientations underlies "normalization." Whereas in our model, neuronal populations that do not prefer the vertical orientation do not receive sufficient feedforward inputs at all, and until the push-pull effect diminishes, excitatory connections from the central population make up for this deficiency. The feedforward model of Barbera et al. [20] obtained similar conclusions as this work, where the phase of the plaid pattern exerted a strong influence on the firing activity of the LGN neurons. The two drifting sinusoidal gratings forming the plaid have the same temporal frequency at this stage, so that the firing pattern does not change throughout the experiment for LGN neurons at a specific location. The superposition of gratings at different temporal frequencies leads to changes in the firing pattern of the LGN over time, and it is interesting to see what effect this will have on cortical activity. We considered the effect of grating superposition on gamma oscillations, and in contrast to previous modeling studies on the stimulus-dependence of gamma oscillations [24, 26–29], we explained the reason for the change in oscillatory properties not mathematically but in terms of tangible patterns of synaptic connectivity, which is more conducive to the understanding of how gamma oscillations characterize visual stimuli in V1.

Biological experiments have demonstrated that some neurons are sensitive to plaids. Bartolo et al. [6] found that plaid pattern presentation resulted in higher firing rates than the grating case at almost all sites. Muir et al. [8] and Guan et al. [9] both reported that many non-directionally regulated V1 neurons responded strongly to plaids. Barbera et al. [20] implemented the modeling of such plaid-preferring neurons in their proposed feedforward model through a special arrangement of LGNs. These plaid-preferring neurons would simplify the interpretation of some visual processes related to texture, and phase sensitivity to plaids would yield new implications for firing patterns, but at the same time, these neurons are easily ignored by traditional methods of mapping receptive fields using oriented stimuli. How to determine the distribution of such neurons within the layer, whether their plaid preference can come from the directionless arrangement of LGN neurons, and what effect it will have on the cross-inhibition and gamma modulation of the remaining orientation-preference neurons are all issues worth discussing.

Although the push-pull organization in the present model does not produce more inhibitory effects on neurons under plaid stimulation, it is equally important not to ignore the role of recurrent connections within the cortex. The normalization neuro-computational model is thought to operate throughout the visual system as well as in many other sensory modalities and brain regions. In this framework, only the optimal grating increases the excitatory input to the neuron as the numerator, whereas both gratings increase the normalization factor as the denominator, and thus the masked grating leads to diminished firing activity [23, 24]. The stable superlinear network (SSN) model also relies on intracortical suppression to account for cross-inhibition, and in addition, this strategy simulates the superlinearization of the firing rate when two low-contrast gratings are superimposed, where the dominant input source shifts from the feed-forward to the intralaminar loop as the stimulus intensity is increased, resulting in the inputs becoming increasingly suppressive [19]. Taking the above into account, the network structure behind these mechanisms needs to be considered and integrated with existing anatomical studies of intracortical connectivity. Questions such as how to generate the desired circuit structure

with known connection rules, how these cross-inhibition strategies will affect the gamma property, and what kind of neural computation is represented by a change in the gamma property are equally worthy of consideration.

5. Conclusions

To investigate the cross-inhibition in V1, we build a large-scale spiking neural network that takes biological details into account. This model successfully simulates the modulation of cortical neuronal responses by the contrast of orthogonal mask gratings: the superimposed gratings lead to a decrease in the firing rate and a large decrease in the gamma band power along with an increase in the peak frequency, which is consistent with the conclusions obtained from previous biological experiments [2, 3, 6, 7, 10–12]. In this paper, we focus on two components that may induce cross-inhibition: the feedforward from LGN and the push-pull organization within L4. The results suggest that the receptive field structure of LGN neurons and the spatial arrangement of cortical neurons receiving feed-forward inputs work together to result in cross-inhibition. Furthermore, to eliminate feedforward effects, we let the two orthogonal gratings that make up the plaid be presented individually and summed the currents so that populations preferred by both orientations obtain the same level of response when their optimal grating is presented alone. We modify the push-pull strength parameter σ, and the results show that, the higher the push-pull strength the higher the neuron firing rate, and at the same time, the network does not produce a cross-inhibition phenomenon, which demonstrates that the push-pull organization alone is not enough to cause a decrease in the firing rate when the gratings are superimposed. Although push-pull organization does not lead to changes in firing rate, it does affect changes in gamma oscillation frequency. Increased push-pull strength leads to fewer inhibitory synapses in this population and more inhibition in neighboring populations with other preferred orientations. Thus, when a single grating is presented, the inhibition within the population is too weak, leading to low oscillation frequencies. Whereas mask gratings lead to an increase in inhibition from neighboring populations resulting in a high oscillation frequency. These results will help to understand the visual processing under multi-input integration and how gamma oscillation characterizes complex texture information.

Use of AI tools declaration

The authors declare they have not used artificial intelligence (AI) tools in the creation of this article.

Acknowledgments

This research was supported by the National Natural Science Foundation of China (Grants Nos. 12272092 and 12332004).

Conflict of interest

Qingyun Wang is an editorial board member for the Electronic Research Archive and was not involved in the editorial review or the decision to publish this article. The authors declare that there are no conflicts of interest.

References

1. M. C. Morrone, D. C. Burr, L. Maffei, Functional implications of cross-orientation inhibition of cortical visual cells. I. neurophysiological evidence, *Proc. R. Soc. B*, **216** (1982), 335–354, https://doi.org/10.1098/rspb.1982.0078
2. G. C. DeAngelis, J. G. Robson, I. Ohzawa, R. D. Freeman, Organization of suppression in receptive fields of neurons in cat visual cortex, *J. Neurophysiol.*, **68** (1992), 144–163. https://doi.org/10.1152/jn.1992.68.1.144
3. N. J. Priebe, D. Ferster, Mechanisms underlying cross-orientation suppression in cat visual cortex, *Nat. Neurosci.*, **9** (2006), 552–561. https://doi.org/10.1038/nn1660
4. M. Popović, A. K. Stacy, M. Kang, R. Nanu, C. E. Oettgen, D. L. Wise, et al., Development of cross-orientation suppression and size tuning and the role of experience, *J. Neurosci.*, **38** (2018), 2656–2670. https://doi.org/10.1523/JNEUROSCI.2886-17.2018
5. H. E. Jones, W. Wang, A. M. Sillito, Spatial organization and magnitude of orientation contrast interactions in primate V1, *J. Neurophysiol.*, **88** (2002), 2796–2808. https://doi.org/10.1152/jn.00403.2001
6. M. J. Bartolo, M. A. Gieselmann, V. Vuksanovic, D. Hunter, L. Sun, X. Chen, et al., Stimulus-induced dissociation of neuronal firing rates and local field potential gamma power and its relationship to the blood oxygen level-dependent signal in macaque primary visual cortex, *Eur. J. Neurosci.*, **34** (2011), 1857–1870. https://doi.org/10.1111/j.1460-9568.2011.07877.x
7. D. L. Ringach, The geometry of masking in neural populations, *Nat. Commun.*, **10** (2019), 4879. https://doi.org/10.1038/s41467-019-12881-4
8. D. R. Muir, P. Molina-Luna, M. M. Roth, F. Helmchen, B. M. Kampa, Specific excitatory connectivity for feature integration in mouse primary visual cortex, *PLoS Comput. Biol.*, **13** (2017), 1–33. https://doi.org/10.1371/journal.pcbi.1005888
9. S. C. Guan, S. H. Zhang, Y. C. Zhang, S. M. Tang, C. Yu, Plaid detectors in macaque V1 revealed by two-photon calcium imaging, *Curr. Biol.*, **30** (2020), 934–940. https://doi.org/10.1016/j.cub.2020.01.005
10. B. Lima, W. Singer, N. H. Chen, S. Neuenschwander, Synchronization dynamics in response to plaid stimuli in monkey V1, *Cereb. Cortex*, **20** (2009), 1556–1573. https://doi.org/10.1093/cercor/bhp218
11. G. Perry, The effects of cross-orientation masking on the visual gamma response in humans, *Eur. J. Neurosci.*, **41** (2015), 1484–1495. https://doi.org/10.1111/ejn.12900
12. B. Wang, C. Han, T. Wang, W. Dai, Y. Li, Y. Yang, et al., Superimposed gratings induce diverse response patterns of gamma oscillations in primary visual cortex, *Sci. Rep.*, **11** (2021), 4941. https://doi.org/10.1038/s41598-021-83923-5
13. C. M. Gray, P. König, A. K. Engel, W. Singer, Oscillatory responses in cat visual cortex exhibit inter-columnar synchronization which reflects global stimulus properties, *Nature*, **338** (1989), 334–337. https://doi.org/10.1038/338334a0
14. C. M. Gray, The temporal correlation hypothesis of visual feature integration: still alive and well, *Neuron*, **24** (1999), 31–47. https://doi.org/10.1016/S0896-6273(00)80820-X

15. P. Uhlhaas, W. Singer, Neuronal dynamics and neuropsychiatric disorders: toward a translational paradigm for dysfunctional large-scale networks, *Neuron*, **75** (2012), 963–980. https://doi.org/10.1016/j.neuron.2012.09.004

16. N. M. Brunet, C. A. Bosman, M. Vinck, M. Roberts, R. Oostenveld, R. Desimone, et al., Stimulus repetition modulates gamma-band synchronization in primate visual cortex, *PNAS*, **111** (2014), 3626–3631. https://doi.org/10.1073/pnas.1309714111

17. P. Fries, Rhythms for cognition: communication through coherence, *Neuron*, **88** (2015), 220–235. https://doi.org/10.1016/j.neuron.2015.09.034

18. C. E. Boudreau, D. Ferster, Short-term depression in thalamocortical synapses of cat primary visual cortex, *J. Neurosci.*, **25** (2005), 7179–7190. https://doi.org/10.1523/JNEUROSCI.1445-05.2005

19. D. Rubin, S. Van Hooser, K. Miller, The stabilized supralinear network: a unifying circuit motif underlying multi-input integration in sensory cortex, *Neuron*, **85** (2015), 402–417. https://doi.org/10.1016/j.neuron.2014.12.026

20. D. Barbera, N. J. Priebe, L. L. Glickfeld, Feedforward mechanisms of cross-orientation interactions in mouse V1, *Neuron*, **110** (2022), 297–311. https://doi.org/10.1016/j.neuron.2021.10.017

21. M. A. Smith, W. Bair, J. A. Movshon, Dynamics of suppression in macaque primary visual cortex, *J. Neurosci.*, **26** (2006), 4826–4834. https://doi.org/10.1523/JNEUROSCI.5542-06.2006

22. M. Koelling, R. Shapley, M. Shelley, Retinal and cortical nonlinearities combine to produce masking in V1 responses to plaids, *J. Comput. Neurosci.*, **25** (2008), 390–400. https://doi.org/10.1007/s10827-008-0086-6

23. M. Carandini, D. J. Heeger, Normalization as a canonical neural computation, *Nat. Rev. Neurosci.*, **13** (2012), 51–62. https://doi.org/10.1038/nrn3136

24. D. J. Heeger, K. O. Zemlianova, A recurrent circuit implements normalization, simulating the dynamics of V1 activity, *PNAS*, **117** (2020), 22494–22505. https://doi.org/10.1073/pnas.2005417117

25. A. Das, S. Ray, Effect of cross-orientation normalization on different neural measures in macaque primary visual cortex, *Cereb. Cortex Comm.*, **2** (2021), tgab009. https://doi.org/10.1093/texcom/tgab009

26. X. Jia, D. Xing, A. Kohn, No consistent relationship between gamma power and peak frequency in macaque primary visual cortex, *J. Neurosci.*, **33** (2013), 17–25. https://doi.org/10.1523/JNEUROSCI.1687-12.2013

27. N. Meneghetti, C. Cerri, E. Tantillo, E. Vannini, M. Caleo, A. Mazzoni, Narrow and broad γ bands process complementary visual information in mouse primary visual cortex, *eNeuro*, **8** (2021). https://doi.org/10.1523/ENEURO.0106-21.2021

28. C. Han, T. Wang, Y. Wu, Y. Li, Y. Yang, L. Li, et al., The generation and modulation of distinct gamma oscillations with local, horizontal, and feedback connections in the primary visual cortex: a model study on large-scale networks, *Neural Plast.*, **2021** (2021), 8874516. https://doi.org/10.1155/2021/8874516

29. X. Gu, F. Han, Z. Wang, K. Kashif, W. Lu, Enhancement of gamma oscillations in E/I neural networks by increase of difference between external inputs, *Electron. Res. Arch.*, **29** (2021), 3227–3241. https://doi.org/10.3934/era.2021035
30. O. J. A. Gonzalez, K. I. van Aerde, H. D. Mansvelder, J. van Pelt, A. van Ooyen, Inter-network interactions: impact of connections between oscillatory neuronal networks on oscillation frequency and pattern, *PLOS ONE*, **9** (2014), 1–16. https://doi.org/10.1371/journal.pone.0100899
31. S. Keeley, A. A. Fenton, J. Rinzel, Modeling fast and slow gamma oscillations with interneurons of different subtype, *J. Neurophysiol.*, **117** (2017), 950–965. https://doi.org/10.1152/jn.00490.2016
32. S. Makovkin, E. Kozinov, M. Ivanchenko, S. Gordleeva, Controlling synchronization of gamma oscillations by astrocytic modulation in a model hippocampal neural network, *Sci. Rep.*, **12** (2022), 6970. https://doi.org/10.1038/s41598-022-10649-3
33. K. Wang, A. Wei, Y. Fu, T. Wang, X. Gao, B. Fu, et al., State-dependent modulation of thalamocortical oscillations by gamma light flicker with different frequencies, intensities, and duty cycles, *Front. Neuroinf.*, **16** (2022). https://doi.org/10.3389/fninf.2022.968907
34. T. W. Troyer, A. E. Krukowski, N. J. Priebe, K. D. Miller, Contrast-invariant orientation tuning in cat visual cortex: thalamocortical input tuning and correlation-based intracortical connectivity, *J. Neurosci.*, **18** (1998), 5908–5927. https://doi.org/10.1523/JNEUROSCI.18-15-05908.1998
35. J. Kremkow, L. U. Perrinet, C. Monier, J. M. Alonso, A. Aertsen, Y. Frégnac, et al., Push-pull receptive field organization and synaptic depression: mechanisms for reliably encoding naturalistic stimuli in V1, *Front. Neural Circuits*, **10** (2016). https://doi.org/10.3389/fncir.2016.00037
36. M. M. Taylor, D. Contreras, A. Destexhe, Y. Frégnac, J. Antolik, An anatomically constrained model of V1 simple cells predicts the coexistence of push–pull and broad inhibition, *J. Neurosci.*, **41** (2021), 7797–7812. https://doi.org/10.1523/JNEUROSCI.0928-20.2021
37. E. A. Allen, R. D. Freeman, Dynamic spatial processing originates in early visual pathways, *J. Neurosci.*, **26** (2006), 11763–11774. https://doi.org/10.1523/JNEUROSCI.3297-06.2006
38. J. Antoĺık, R. Cagnol, T. Rozsa, C. Monier, Y. Frégnac, A. P. Davison, A comprehensive data-driven model of cat primary visual cortex, *bioRxiv*, 2023. https://doi.org/10.1101/416156
39. N. Fourcaud-Trocmé, D. Hansel, C. van Vreeswijk, N. Brunel, How spike generation mechanisms determine the neuronal response to fluctuating inputs, *J. Neurosci.*, **23** (2003), 11628–11640. https://doi.org/10.1523/JNEUROSCI.23-37-11628.2003
40. J. Antolik, J. Bednar, Development of maps of simple and complex cells in the primary visual cortex, *Front. Comput. Neurosci.*, **5** (2011). https://doi.org/10.3389/fncom.2011.00017
41. T. Binzegger, R. J. Douglas, K. A. C. Martin, A quantitative map of the circuit of cat primary visual cortex, *J. Neurosci.*, **24** (2004), 8441–8453. https://doi.org/10.1523/JNEUROSCI.1400-04.2004
42. A. Stepanyants, J. A. Hirsch, L. M. Martinez, Z. F. Kisvárday, A. S. Ferecskó, D. B. Chklovskii, Local potential connectivity in cat primary visual cortex, *Cereb. Cortex*, **18** (2007), 13–28. https://doi.org/10.1093/cercor/bhm027
43. L. Chariker, R. Shapley, L. S. Young, Orientation selectivity from very sparse lgn inputs in a comprehensive model of macaque V1 cortex, *J. Neurosci.*, **36** (2016), 12368–12384. https://doi.org/10.1523/JNEUROSCI.2603-16.2016

44. L. Chariker, R. Shapley, L. S. Young, Rhythm and synchrony in a cortical network model, *J. Neurosci.*, **38** (2018), 8621–8634. https://doi.org/10.1523/JNEUROSCI.0675-18.2018

45. J. A. Henrie, R. Shapley, Lfp power spectra in V1 cortex: the graded effect of stimulus contrast, *J. Neurosci.*, **94** (2005), 479–490. https://doi.org/10.1152/jn.00919.2004

46. S. Katzner, I. Nauhaus, A. Benucci, V. Bonin, D. L. Ringach, M. Carandini, Local origin of field potentials in visual cortex, *Neuron*, **61** (2009), 35–41. https://doi.org/10.1016/j.neuron.2008.11.016

47. G. T. Einevoll, C. Kayser, N. K. Logothetis, S. Panzeri, Modelling and analysis of local field potentials for studying the function of cortical circuits, *Nat. Rev. Neurosci.*, **14** (2013), 770–785. https://doi.org/10.1038/nrn3599

48. T. V. Ness, M. W. H. Remme, G. T. Einevoll, Active subthreshold dendritic conductances shape the local field potential, *J. Physiol.*, **594** (2016), 3809–3825. https://doi.org/10.1113/JP272022

49. A. Mazzoni, H. Lindén, H. Cuntz, A. Lansner, S. Panzeri, G. T. Einevoll, Computing the local field potential (lfp) from integrate-and-fire network models, *PLoS Comput. Biol.*, **11** (2015), e1004584. https://doi.org/10.1371/journal.pcbi.1004584

50. A. V. Rangan, L. S. Young, Emergent dynamics in a model of visual cortex, *J. Comput. Neurosci.*, **35** (2013), 155–167. https://doi.org/10.1007/s10827-013-0445-9

51. L. Chariker, L. S. Young, Emergent spike patterns in neuronal populations, *J. Comput. Neurosci.*, **38** (2015), 203–220. https://doi.org/10.1007/s10827-014-0534-4

52. G. Blasdel, Orientation selectivity, preference, and continuity in monkey striate cortex, *J. Neurosci.*, **12** (1992), 3139–3161. https://doi.org/10.1523/JNEUROSCI.12-08-03139.1992

53. M. Whittington, R. Traub, N. Kopell, B. Ermentrout, E. Buhl, Inhibition-based rhythms: experimental and mathematical observations on network dynamics, *Int. J. Psychophysiol.*, **38** (2000), 315–336. https://doi.org/10.1016/S0167-8760(00)00173-2

54. C. Börgers, S. Epstein, N. J. Kopell, Background gamma rhythmicity and attention in cortical local circuits: a computational study, *PNAS*, **102** (2005), 7002–7007. https://doi.org/10.1073/pnas.0502366102

AIMS Press